Calibration of higher eigenmode spring constants of atomic force microscope cantilevers

Jose R Lozano[1]**, Daniel Kiracofe**[2]**, John Melcher**[2]**, Ricardo Garcia**[1] **and Arvind Raman**[2]

[1] IMM—Instituto de Microelectrónica de Madrid (CNM-CSIC), Isaac Newton 8, PTM, E-28760 Tres Cantos, Madrid, Spain
[2] Birck Nanotechnology Center and School of Mechanical Engineering, Purdue University, West Lafayette, IN 47904-2088, USA

E-mail: raman@purdue.edu

Abstract
Standard spring constant calibration methods are compared when applied to higher eigenmodes of cantilevers used in dynamic atomic force microscopy (dAFM). Analysis shows that Sader's original method (Sader *et al* 1999 *Rev. Sci. Instrum.* **70** 3967–9), which relies on *a priori* knowledge of the eigenmode shape, is poorly suited for the calibration of higher eigenmodes. On the other hand, the thermal noise method (Hutter and Bechhoefer 1993 *Rev. Sci. Instrum.* **64** 1868–73) does not require knowledge of the eigenmode and remains valid for higher eigenmodes of the dAFM probe. Experimental measurements of thermal vibrations in air for three representative cantilevers are provided to support the theoretical results.

1. Introduction

Atomic force microscopy (AFM) stands out among other microscopy techniques for its capability to render images of heterogeneous surfaces with nanometric resolution [1–3]. In recent years several attempts have been proposed to also convert AFM into an analytical tool, able to measure quantitatively and precisely the local properties. The problem of force inversion (i.e. to extract the actual value of the interaction between tip and sample from experimental observables) has been solved under different approximations in amplitude- [4–7] and frequency-modulation [8, 9] modes.

To combine both quantitative material information and high resolution imaging a number of groups have opted for the excitation and/or detection of higher harmonics [10] of the cantilever motion and/or higher eigenmodes [11] which are related to other flexural [12] or torsional [13] resonances of the probe. However, the quest for quantitative information in AFM greatly depends on accurate calibration of the relevant spring constant(s) for the application. Quasi-static AFM modes require the static spring constant, i.e. the constant relating a point-load applied at the tip and the resulting deflection of the tip, to be calibrated [14]. Dynamic AFM modes require

the equivalent spring constants of the participating eigenmodes to be calibrated. However, the close similarity between the spring constant of the fundamental eigenmode and the static spring constant [15] has resulted in the two rarely being distinguished from one another in the literature. The evolution of dynamic AFM to incorporate higher eigenmodes requires that distinction is made between the static spring constant, k_{static}, and the equivalent spring constant of higher eigenmodes, k_n ($n > 1$). Moreover, we must reconsider calibration methods, which were originally developed specifically to calibrate k_{static}, and how they can be modified to produce k_n [16].

Several methods have been suggested to calibrate k_{static} [17–31], although two of them have been particularly popular [32]. The first was proposed by Sader [19]. Remarkably, this method uses the predicted hydrodynamic damping affecting a rectangular AFM probe immersed in a fluid to calibrate k_{static} in terms of the measured quality factor and resonance frequency, as well as the geometrical dimensions of the beam. On the other hand the thermal noise method, originally proposed by Hutter and Bechhoefer [17] but later modified by Butt and Jaschke [16], takes advantage of the equipartition theorem which relates the thermal fluctuations

of the cantilever to the equilibrium temperature of the surrounding fluid through k_{static}. While these methods are mostly used for calibration of the fundamental eigenmode, it remains unclear whether or not these methods can be extended to higher eigenmodes.

In this paper, we investigate the calibration of higher eigenmodes through adaptations of the Sader method and the thermal noise method. We find considerable limitations to the Sader method for calibrating higher eigenmodes due to the necessity of *a priori* knowledge of the eigenmode. Specifically, the sensitivity of higher eigenmodes to the tip mass and the cantilever geometry introduces large errors in the Sader method when applied to higher eigenmodes [33]. We find that thermal calibration is much more amenable to the calibration of higher eigenmodes, as long as the resonance frequencies, f_n, are adequately spaced. Specifically, the spacing of the resonances, $f_2 - f_1$, should be greater than their bandwidths, f_n/Q_n, with Q_n the eigenmode quality factor. Experimental results are presented for three representative cantilevers: a tipped rectangular cantilever, a tipless rectangular cantilever, and a tipless picket-shaped cantilever.

2. Theory

We begin with the application of standard beam theory to demonstrate the influence of a particle mass at the free end of a uniform rectangular cantilever in higher eigenmode spring constants. The Euler–Bernoulli partial differential equation (PDE) describes the motion in time of a one-dimensional beam in the presence of external forces, among which we will only consider the hydrodynamic loading of the surrounding fluid. In the Fourier domain it is expressed as [34],

$$\frac{EI}{L^4} W_{xxxx}(x, \omega) - \rho_c bh\omega^2 W(x, \omega) = \frac{\pi}{4} \rho_f b^2 \omega^2 \Gamma(\omega) W(x, \omega)$$
(1)

where $W(x, \omega)$ is the Fourier transform of the out-of-plane displacement of a beam element, placed in its longitudinal normalized coordinate, x. E is the Young's modulus, I is the moment of inertia and L the length of the cantilever. The angular frequency is referred to as ω, while partial derivatives with respect to x are denoted by $(\cdot)_x$. The cantilever density, width and thickness are denoted respectively by ρ_c, b and h. The right-hand side of equation (1) represents the hydrodynamic loading, with ρ_f and $\Gamma(\omega)$, respectively, the surrounding fluid density and the (complex) hydrodynamic function of the problem, as defined in [34].

We introduce the tip effect approximated as a particle mass, m_{tip}, which leads to a shear force balance at the free end of the cantilever. The boundary conditions of a beam clamped at $x = 0$, and supporting a mass particle at $x = 1$ are given by [33, 35, 36]

$$W(0, \omega) = W_x(0, \omega) = W_{xx}(1, \omega) = 0;$$
$$\frac{EI}{L^3} W_{xxx}(1, \omega) = -m_{tip}\omega^2 W(1, \omega).$$
(2)

The eigenmodes, $\Phi_n(x)$, and the characteristic equation for the eigenvalues, α_n, follow from separation of variables

in the Euler–Bernoulli PDE, equation (1), and imposition of the boundary conditions, equations (2). Because the damping in air is small, the undamped eigenmodes and the damped eigenmodes are nearly identical [37]. Therefore, the imaginary part of the hydrodynamic function can be neglected in equation (1), yielding

$$\Phi_n(x; m^*) = \cos(\alpha_n x) - \cosh(\alpha_n x)$$
$$- \frac{\cos(\alpha_n) + \cosh(\alpha_n)}{\sin(\alpha_n) + \sinh(\alpha_n)} (\sin(\alpha_n x) - \sinh(\alpha_n x))$$
(3)

where α_n is a solution of

$$1 + \cos\alpha_n \cosh\alpha_n + m^*\alpha_n(\sinh\alpha_n \cos\alpha_n - \sin\alpha_n \cosh\alpha_n)$$
$$= 0$$
(4)

where $m^* \equiv m_{tip}/(m_{beam} + m_{hydro})$ is the reduced or dimensionless tip mass, and with $m_{beam} \equiv \rho_c bhL$ and $m_{hydro} \equiv \pi\rho_f b^2 L \, \text{Re}[\Gamma(\omega)]/4$ the cantilever and hydrodynamic added masses, respectively. Here, the real part of the hydrodynamic function is denoted by $\text{Re}[\Gamma]$. Equations (3) and (4) show that the shapes of the eigenmodes, $\Phi_n(x; m^*)$, are determined by their eigenvalues, α_n, which in turn are determined by the value of m^*. We have omitted the dependence of α_n on m^*, $\alpha_n(m^*)$, for simplicity of notation. At this point we would like to remark that the value of m^* depends on the eigenmode considered because the hydrodynamic added mass, m_{hydro}, is frequency dependent, according to Sader's theory. However, for cantilevers immersed in air, m_{hydro} is negligible, which leads to $m^* = m_{tip}/m_{beam}$, regardless of the eigenmode number. We will assume this situation during the present work.

Here we are concerned with the measurement of the equivalent spring constant related to the tip deflection of the nth eigenmode, k_n. Accordingly, we apply the energy equivalence principle [15], relating k_n to Φ_n (the prime denotes total derivative with respect to x),

$$k_n(m^*) = \frac{EI}{L^3} \frac{\int_0^1 dx \, [\Phi_n''(x; m^*)]^2}{[\Phi_n(1; m^*)]^2}.$$
(5)

From the above results we deduce that when the eigenmode shapes are modified by m^*, the equivalent spring constants will be affected too. On the other hand, if $m^* = 0$ we recover the eigenmode shapes and equivalent spring constants corresponding to rectangular tipless cantilevers [15].

Figure 1(a) shows the dependence of the ratio k_n/k_{static} for eigenmodes $n = 1, 2$ with respect to the reduced mass, m^*, with $k_{static} \equiv 3EI/L^3$ (constant) the cantilever static spring constant [38]. While k_1/k_{static} is found to slowly decrease from 1.03 to 1.00 when varying m^* between 0 and 0.2, k_2/k_{static} dramatically increases from 40.2 to 125. Thus, the presence of a tip mass at the free end of the cantilever does not modify the first eigenmode spring constant significantly, but causes major changes in k_2. For a tip mass that is 10% of the cantilever mass, $m^* = 0.1$, the equivalent spring constant will be $k_2 = 74.9k_{static}$. The increase in k_2 with respect to m^* occurs primarily because $\Phi_2(1; m^*)$ becomes small as $\Phi_2(x; m^*)$ begins to resemble the fundamental eigenmode of a clamped–pinned beam for large values of m^*. On the other hand, $\Phi_1(x; m^*)$ will approach the profile of a cantilever with a static point-load applied at the free end, and thus $k_1 \to k_{static}$.

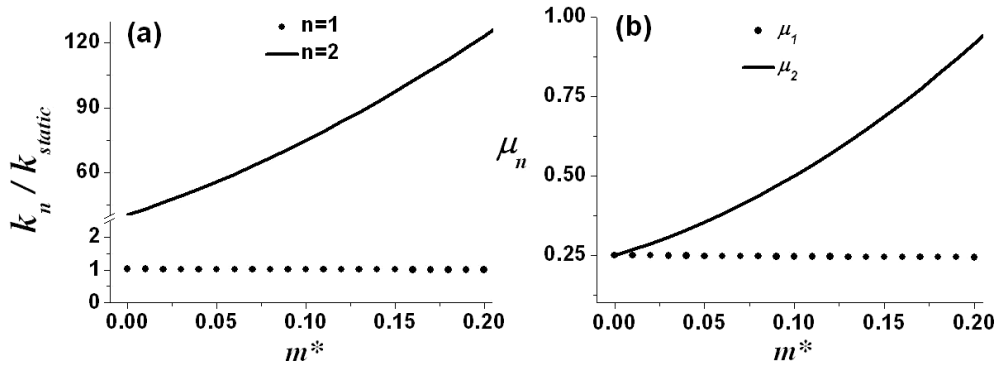**Figure 1.** (a) Normalized equivalent spring constants, k_n/k_{static}, and (b) effective mass factors, μ_n, for first (circles) and second (solid line) eigenmodes are plotted with respect to the reduced mass, m^*.

Once we have calculated the eigenmodes of the problem, $\Phi_n(x; m^*)$, we can implement the general form of the Sader formula to calculate the fundamental and higher eigenmodes equivalent spring constant, $n \geqslant 1$,

$$k_{n\,\text{Sader}} = \mu_n \frac{\pi}{4} Lb^2 \rho_f \,\text{Im}[\Gamma(\omega_n)]\omega_n^2 Q_n \qquad (6)$$

where ω_n and Q_n are, respectively, the measured resonance frequency and quality factor of the eigenmode considered. The imaginary part of the hydrodynamic function is denoted by $\text{Im}[\Gamma]$. The effective mass factor of the beam, μ_n, is defined as

$$\mu_n(m^*) \equiv \frac{\int_0^1 \mathrm{d}x \, [\Phi_n(x; m^*)]^2}{[\Phi_n(1; m^*)]^2}, \qquad (7)$$

and will depend on the tip mass through m^*. Note that if in equation (6) μ_n is set to $\mu_{static} = 0.2427$ and $n = 1$, we recover the original Sader formula for k_{static} [19]. On the other hand, we would like to remark that calibration of the tipless rectangular cantilever's first mode spring constant technically requires the application of equation (6) with $n = 1$ and $\mu_1 = 0.25$; however, the difference is clearly small.

In figure 1(b) the dependence of μ_n for $n = 1, 2$ with respect to m^* is shown. As with the equivalent spring constant, the first eigenmode effective mass factor, μ_1, tends to μ_{static} in the limiting case of large m^*. However, μ_2 increases from 0.25 to 1 when m^* changes from 0 to 0.2. Consequently, equations (6) and (7) imply that the application of the original Sader formula to determine k_2 would entail an error of about 100% for a tip mass $m_{tip} = 0.1m_{beam}$.

The correct application of equation (6) would involve an accurate knowledge of the eigenmode shape (equation (3)) or of the reduced mass, m^*. Because this is rarely the case for most commercially available probes, we recommend use of the thermal noise method proposed by Hutter and Bechhoefer to calibrate spring constants of higher eigenmodes of non-rectangular and/or tipped cantilevers. This method provides the spring constant of a given eigenmode by measuring the temperature and thermal fluctuations under the desired resonance in the cantilever response power spectral density (PSD).

Most AFM experimental setups use a quadrature photodiode system [39], which measures the bending angle (slope) of the cantilever rather than its deflection or velocity. Thus, additional optical lever sensitivity calibration must be performed to relate the bending angle at the laser spot location to the deflection of the tip in each eigenmode. This can be performed either theoretically, with knowledge of the shape of the eigenmode [16, 36, 40], or experimentally [41]. However, in our experimental setup (see section 3), laser Doppler vibrometry was used to measure the cantilever's velocity directly, which did not require the optical lever sensitivity calibration [42]. Consequently, in order to apply the thermal noise method to higher eigenmodes, the equipartition theorem had to be applied to the velocity, yielding the eigenmode effective mass instead of the spring constant itself [43]. Finally the latter could be calculated by mere multiplication by ω_n^2,

$$k_{n\,\text{thermal}} = \frac{k_B T}{\langle q_n^2 \rangle} = \frac{\omega_n^2 k_B T}{\langle \dot{q}_n^2 \rangle} \qquad (8)$$

where q_n is the modal projection of the tip deflection, and where the symbols $\langle q \rangle$ and $\dot{q}$ denote, respectively, statistical average and temporal derivative of q. The Boltzmann constant is denoted by k_B, while T represents the equilibrium temperature.

3. Methodology

To compare the Sader and thermal noise methods, thermal vibration time series were measured by laser Doppler vibrometry (Polytec MSA-400 Micro System Analyzer from Polytec Gmbh, Waldbronn, Germany, laser spot size approximately 1 μm) at the free end of three different cantilevers: tipped rectangular, tipless rectangular and tipless picket, respectively. Their manufacturer, model, type, length and width are listed in table 1 (see figure 2 for scanning electron microscopy (SEM) images of the three cantilevers). For each cantilever, n_r velocity time series containing N points and sampled at a frequency f_s (see table 1) were measured. The PSD of the velocity time series was estimated using Welch's periodogram method [44]. Each time series was divided into n_{seg} segments and the overall estimate of the PSD of each time series was taken as the average of the estimates from each segment. The sampling frequency f_s was selected based on each cantilever's second natural frequency and the number of points was chosen such that the number of points inside
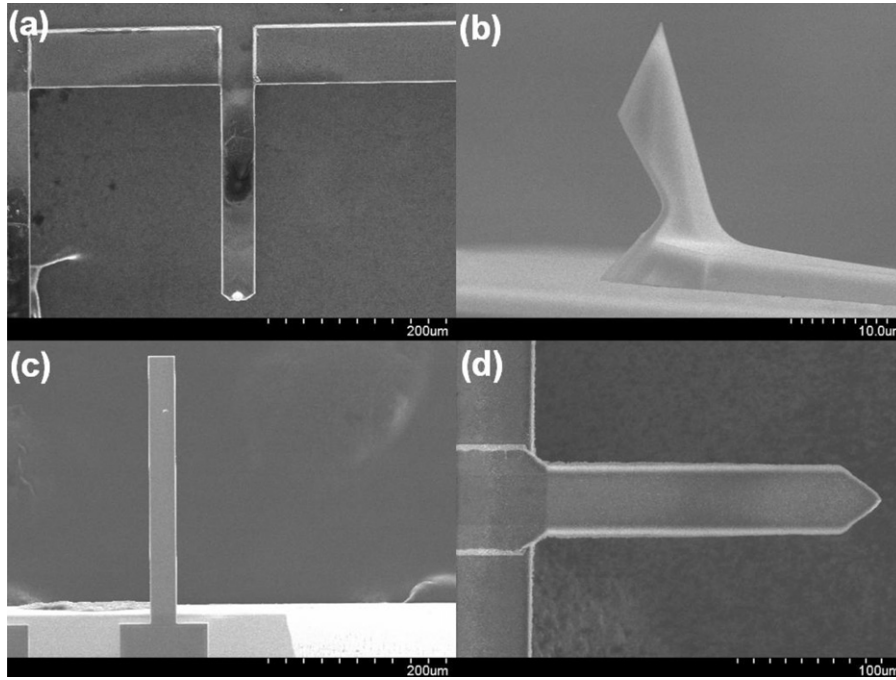
Figure 2. SEM images of the cantilevers discussed in section 4. (a) Planar view of cantilever 1 (tipped rectangular). (b) Detail of the tip from cantilever 1. (c) Planar view of cantilever 2 (tipless rectangular). (d) Planar view of cantilever 3 (tipless picket).

Table 1. Manufacturer specifications and PSD parameters for the AFM probes analyzed in this paper. L and b are, respectively, the cantilever length and width. For each cantilever, n_r time series containing N data points were sampled at a frequency f_s. Each time series was then divided into n_{seg} segments and the PSD of each time series was estimated as the average of the PSD of each segment.

Cantilever	Manufacturer	Model	Type	L (μm)	b (μm)	N	n_{seg}	f_s (MHz)	n_r
1	Mikromasch	NSC12 F	Tipped	250	35	2^{21}	128	1.024	5
2	Sandia	CADP	Tipless	300	29	2^{19}	128	0.512	4
3	AppNano	Forta TL	Picket	213	36	2^{23}	128	2.560	5

the resonance bandwidth is approximately the same for each cantilever (see table 1 for the parameters used to calculate the PSD).

Figure 3(a) depicts the experimental PSD velocity thermal fluctuations measured at the free end of a tipped cantilever. The first two flexural resonances are marked by arrows and also enlarged in figures 3(b) and (c) respectively. Other peaks in the spectrum correspond to spurious resonances and electronic or mechanical noise. To estimate the thermal noise contained in the desired eigenmode resonance, the latter was normalized to its maximum, PSD_{max}, and fitted to the PSD of a single harmonic oscillator (see figures 3(b) and (c)). The quality factor, Q_n, and resonance frequency, $f_n = \omega_n/2\pi$, were obtained as fitting parameters. In order to avoid the influence from the noise floor, the eigenmode's thermal fluctuations in velocity were determined as the integral of the fitted PSD,

$$\langle \dot{q}_n^2 \rangle = \text{PSD}_{max} \int_0^\infty df \frac{(f/f_n)^2}{Q_n^2[1-(f/f_n)^2]^2 + (f/f_n)^2}. \quad (9)$$

Once the quality factor, resonance frequency and thermal fluctuations were obtained for each eigenmode, Sader and thermal noise methods were applied for both eigenmodes of all the three cantilevers. In particular, for the Sader method equation (6) was used with $\mu_n = 0.25$ and $n = 1, 2$

respectively, yielding the first and second eigenmode equivalent spring constants corresponding to eigenmode shapes where $m^* = 0$. In that way, k_1 and k_2 were obtained from the original Sader method, rather than k_{static}. Finally, to estimate k_n by means of the thermal noise method, equations (8) and (9) were used.

Sader's method is frequently applied to a quality factor obtained from a driven/forced response (tuning curves), whereas in this experiment a quality factor obtained from a thermal response is used. These quality factors should theoretically be the same [19]. We have confirmed that these are similar by comparing the thermal and forced response for cantilever 3. An agreement in quality factor of 7% (not shown) was found between the two values.

A third method is provided as a reference to verify the experimental procedure and that the spring constants predicted from the thermal noise protocol are correct. This was achieved by using the scanning laser Doppler vibrometer to measure the PSD at multiple points along the x-axis of the cantilever (see insets in figure 3(a) for the normalized PSD profile along cantilever 1—tipped rectangular—at its first two eigenmodes respectively). Then, the experimental data were fitted to the square of the eigenmode given in equation (3) with $n = 2$, to directly determine the eigenvalue α_2. From this and
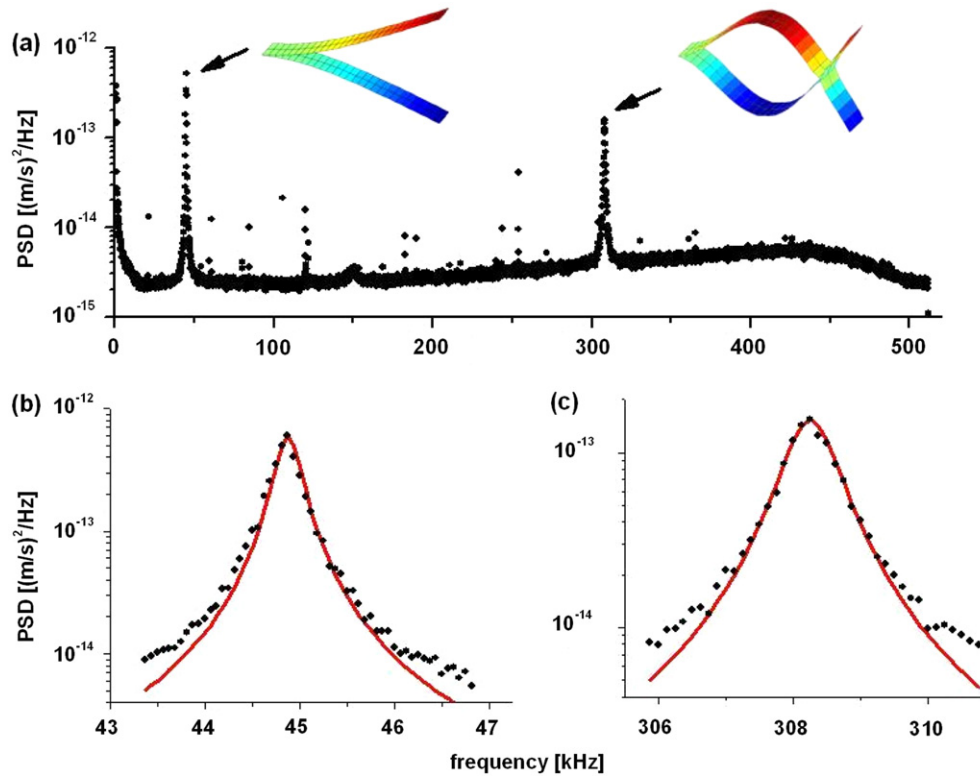
Figure 3. (a) Velocity power spectral density (PSD) under thermal motion of cantilever 1 (tipped rectangular). The first two flexural resonances are marked by arrows and enlarged in (b) first eigenmode and (c) second eigenmode. The solid lines in (b) and (c) correspond to the fitting performed on each resonance to a single harmonic oscillator, with the eigenmode resonance frequency and quality factor as the only free parameters. The other two cantilevers yielded similar frequency responses (see tables 1 and 2 for specific details). The insets in figure 3(a) show the PSD profiles measured along cantilever 1's *x*-axis, normalized to the value at the free end, for the first and second eigenmodes.

(This figure is in colour only in the electronic version)

Table 2. First and second eigenmode resonance frequencies, f_n, quality factors, Q_n, and equivalent spring constants, calibrated by thermal noise, $k_{n,\text{thermal}}$, and Sader methods, $k_{n,\text{Sader}}$, for the cantilevers described in table 1. Error bars are calculated as the standard deviation of the estimates, obtained from the different time series taken for each cantilever. For the resonance frequency, error bars were calculated as the maximum between half of the PSD frequency resolution, $\Delta f = f_s n_{\text{seg}}/N$, and the standard deviation.

Cantilever	f_1 (kHz)	Q_1	$k_{1,\text{thermal}}$ (N m^{-1})	$k_{1,\text{Sader}}$ (N m^{-1})	f_2 (kHz)	Q_2	$k_{2,\text{thermal}}$ (N m^{-1})	$k_{2,\text{Sader}}$ (N m^{-1})
1	44.88 ± 0.03	150 ± 20	1.21 ± 0.04	1.2 ± 0.1	308.20 ± 0.08	390 ± 40	76 ± 2	50 ± 5
2	33.00 ± 0.06	82 ± 8	0.46 ± 0.02	0.43 ± 0.04	204.50 ± 0.06	270 ± 30	22.6 ± 0.5	19 ± 2
3	72.62 ± 0.02	139 ± 7	1.64 ± 0.04	1.63 ± 0.08	454.6 ± 0.1	420 ± 20	55 ± 2	71 ± 4

equation (5), the value of k_2/k_1 was calculated, and denoted by $k_2/k_{1,\text{fit}}$ (see [36] for details of the method). Note that, while this method is using thermal noise measurements, it is the noise profile along the beam, rather than the overall magnitude at the cantilever free end, that ultimately determines k_2. Also, this method is not practical for implementation on an AFM, but does provide a useful check of our experiments.

Finally, the SEM images in figure 2 were used to estimate $m^* = m_{\text{tip}}/m_{\text{beam}}$. This estimate is denoted m^*_{SEM} and is calculated from the ratio of the volumes of tip and cantilever, assuming the same mass density in both elements. For the picket cantilever, m^*_{SEM} (negative) is estimated from the top view as the effective area removed from a rectangular beam with the same length. For the tipped cantilever the tip is approximated as half a cone and is estimated

from top, side, and front views. From this estimate, it is possible to numerically compute the ratio $k_2/k_1(m^*_{\text{SEM}})$ from equations (3)–(5).

4. Results and conclusions

The main results are summarized in table 2. Equivalent modal spring constants, k_1 and k_2, calculated by the thermal noise and Sader methods, as well as resonance frequencies and quality factors for the first and second eigenmodes, are shown for the three cantilevers. The corresponding value of each magnitude was calculated as the mean of the results obtained in the n_r replicates, while the random error was characterized by the standard deviation. The differences between stiffnesses from Sader's method and the thermal method reported in

Table 3. Thermal noise method versus Sader method spring constant calibration comparison for both eigenmodes, $n = 1, 2$. The first and third columns show the $k_{n,\mathrm{Sader}}/k_{n,\mathrm{thermal}}$ ratio from table 1 values. The second and fourth columns list the normalized deviation between the thermal noise and Sader methods, $R_n = (k_{n,\mathrm{thermal}} - k_{n,\mathrm{Sader}})/\Delta k_{n,\mathrm{Sader}}$, with $\Delta k_{n,\mathrm{Sader}}$ representing the error bars for $k_{n,\mathrm{Sader}}$ from table 1.

Cantilever	$k_{1,\mathrm{thermal}}/k_{1,\mathrm{Sader}}$	R_1	$k_{2,\mathrm{thermal}}/k_{2,\mathrm{Sader}}$	R_2
1	1.03 ± 0.09	0.1	1.5 ± 0.1	5.2
2	1.07 ± 0.07	0.7	1.2 ± 0.2	1.8
3	1.00 ± 0.04	0.1	0.78 ± 0.05	−4.0

table 2 are summarized in table 3. The first column shows that, regardless of the cantilever type, both methods agree within 7% for k_1, and the second column indicates that the difference is not statistically significant (i.e. the difference in the means is small compared to the standard deviations)—a result previously shown by other groups [42, 45, 46]. However, differences of up to 50% are observed when comparing the calibration protocols for k_2 [33] and these are statistically significant (i.e. the difference in the means is large compared to the standard deviation). Moreover, the greatest differences happen for cantilever 1 (tipped rectangular, 50% error), while cantilever 2 (tipless rectangular) exhibits a deviation of about 20%. Finally, cantilever 3 (tipless picket) presents a 22% error between the two methods in the second eigenmode spring constant. Our results show a clear deviation between the thermal noise and Sader methods for the second eigenmode depending on the type of cantilever considered: the tipped rectangular one presents greater deviations than the tipless picket-shaped one, and the latter shows greater deviations than the tipless rectangular one.

Table 4 shows k_2/k_1 ratios calculated from table 2 for Sader and thermal methods, compared to the values calculated by the third method, $k_2/k_{1,\mathrm{fit}}$. It can be seen that $k_2/k_{1,\mathrm{fit}}$ and $k_2/k_{1,\mathrm{thermal}}$ agree within less than 12% error, while differences up to 35% are observed between k_2/k_1 and $k_2/k_{1,\mathrm{Sader}}$, confirming our experimental results.

Finally, the values for m^* estimated from the SEM images in figure 2, m^*_{SEM}, and the theoretical ratio, $k_2/k_1(m^*_{\mathrm{SEM}})$, are presented in the last two columns of table 4. Theoretical and thermally measured k_2/k_1 ratios agree within 20% in all the cases, the main sources of error being attributed to the non-uniformity of the beam thickness along its length [33] as well as the approximation of the mass inhomogeneity as a particle at the free end. However, differences up to 60% are observed between $k_2/k_1(m^*_{\mathrm{SEM}})$ and $k_2/k_{1,\mathrm{Sader}}$.

The data in tables 2–4 demonstrate that there are important limitations to the Sader method when applied to higher eigenmodes due to their sensitivity to mass inhomogeneities at the free end, such as tip mass or picket geometry. On the other hand, the thermal noise method does not require knowledge of the eigenmode shape, and, as a result, is better suited for the calibration of higher eigenmodes. Furthermore, table 4 shows that mass inhomogeneities have a strong effect on the spring constant ratio k_2/k_1, a fact which may be important for probe selection in AFM methods which utilize the multiple eigenmodes [47, 48].

In conclusion, we have compared the two most popular calibration methods, Sader and thermal noise methods, and their application to higher eigenmode spring constant determination in air, by means of laser Doppler vibrometry. Results were presented for AFM probes with two subtle, but common, mass inhomogeneities (tip mass and picket shape). We have found both protocols to agree within 7% in the first eigenmode, while the effect of mass inhomogeneities could lead to errors of up to 60% in the second eigenmode when using Sader's method, due to deviations in the eigenmode shape with respect to tipless rectangular cantilever eigenmodes. Because the Sader method relies on geometric aspects and strictly considers tipless rectangular cantilevers, we propose the thermal noise method to be the method of choice when calibrating the spring constant of AFM probe higher eigenmodes.

Acknowledgments

References

[1] Kuna J J, Voitchovsky K, Singh C, Jiang H, Mwenifumbo S, Ghorai P K, Stevens M M, Glotzer S C and Stellacci F 2009 *Nat. Mater.* **8** 837–42

Table 4. First and second eigenmode equivalent spring constant ratios, k_2/k_1, from thermal noise and Sader calibration methods, are compared with ratios predicted by equation (5), in two different ways. $k_2/k_1(m^*_{\mathrm{SEM}})$ is calculated by estimating the reduced tip mass, m^*, as the ratio of tip and cantilever volumes, from the SEM images in figure 2. $k_2/k_{1,\mathrm{fit}}$ is calculated by fitting measured second eigenmode shapes to equation (3), to determine the eigenvalue α_2. Then, equation (5) is applied to calculate k_2/k_1. The brackets indicate upper and lower bounds of the corresponding estimate.

Cantilever	$k_2/k_{1,\mathrm{thermal}}$	$k_2/k_{1,\mathrm{Sader}}$	$k_2/k_{1,\mathrm{fit}}$	$k_2/k_1\,(m^*_{\mathrm{SEM}})$	m^*_{SEM}
1	62.8	41.7	57.8	(45.0, 65.8)	(0.02, 0.08)
2	49.1	44.2	43.8	39.0	0.00
3	33.5	43.6	32.4	27.7	−0.06

[2] Dong M D, Husale S and Sahin O 2009 *Nat. Nanotechnol.* **4** 514–7

[3] Garcia R, Magerle R and Perez R 2007 *Nat. Mater.* **6** 405–11

[4] Holscher H 2006 *Appl. Phys. Lett.* **89** 123109

[5] Lee M H and Jhe W H 2006 *Phys. Rev. Lett.* **97** 036104

[6] Hu S Q and Raman A 2008 *Nanotechnology* **19** 375704

[7] Katan A J, van Es M H and Oosterkamp T H 2009 *Nanotechnology* **20** 165703

[8] Durig U 1999 *Appl. Phys. Lett.* **75** 433–5

[9] Sader J E and Jarvis S P 2004 *Appl. Phys. Lett.* **84** 1801–3

[10] Legleiter J, Park M, Cusick B and Kowalewski T 2006 *Proc. Natl Acad. Sci.* **103** 4813–8

[11] Sugimoto Y, Innami S, Abe M, Custance O and Morita S 2007 *Appl. Phys. Lett.* **91** 093120

[12] Stark M, Stark R W, Heckl W M and Guckenberger R 2002 *Proc. Natl Acad. Sci.* **99** 8473–8

[13] Sahin O, Magonov S, Su C, Quate C F and Solgaard O 2007 *Nat. Nanotechnol.* **2** 507–14

[14] Butt H J, Cappella B and Kappl M 2005 *Surf. Sci. Rep.* **59** 1–152

[15] Melcher J, Hu S and Raman A 2007 *Appl. Phys. Lett.* **91** 053101

[16] Butt H J and Jaschke M 1995 *Nanotechnology* **6** 1–7

[17] Hutter J L and Bechhoefer J 1993 *Rev. Sci. Instrum.* **64** 1868–73

[18] Cleveland J P, Manne S, Bocek D and Hansma P K 1993 *Rev. Sci. Instrum.* **64** 403–5

[19] Sader J E, Chon J W M and Mulvaney P 1999 *Rev. Sci. Instrum.* **70** 3967–9

[20] Snow D E, Weeks B L, Kim D J, Pitchimani R and Hope-Weeks L J 2008 *Rev. Sci. Instrum.* **79** 083706

[21] Vakarelski I U, Edwards S A, Dagastine R R, Chan D Y C, Stevens G W and Grieser F 2007 *Rev. Sci. Instrum.* **78** 116102

[22] Degertekin F L, Hadimioglu B, Sulchek T and Quate C F 2001 *Appl. Phys. Lett.* **78** 1628–30

[23] Maeda N and Senden T J 2000 *Langmuir* **16** 9282–6

[24] Torii A, Sasaki M, Hane K and Okuma S 1996 *Meas. Sci Technol.* **7** 179–84

[25] Cumpson P J, Zhdan P and Hedley J 2004 *Ultramicroscopy* **100** 241–51

[26] Gibson C T, Watson G S and Myhra S 1996 *Nanotechnology* **7** 259–62

[27] Hazel J L and Tsukruk V V 1999 *Thin Solid Films* **339** 249–57

[28] Langlois E D, Shaw G A, Kramar J A, Pratt J R and Hurley D C 2007 *Rev. Sci. Instrum.* **78** 093705

[29] Notley S M, Biggs S and Craig V S J 2003 *Rev. Sci. Instrum.* **74** 4026–32

[30] Rabinovich Y I and Yoon R H 1994 *Langmuir* **10** 1903–9

[31] Senden T and Ducker W 1994 *Langmuir* **10** 1003–4

[32] Cook S M, Schaffer T E, Chynoweth K M, Wigton M, Simmonds R W and Lang K M 2006 *Nanotechnology* **17** 2135–45

[33] Allen M S, Sumali H and Penegor P C 2009 *Trans. ASME, J. Dyn. Syst. Meas. Control* **131** 06401

[34] Sader J E 1998 *J. Appl. Phys.* **84** 64–76

[35] Kokavecz J and Mechler A 2008 *Phys. Rev.* B **78** 172101

[36] Kiracofe D and Raman A 2010 *J. Appl. Phys.* **107** 033506–9

[37] Woodhouse J 1998 *J. Sound Vib.* **215** 547–69

[38] Sarid D 1991 *Scanning Force Microscopy* (New York: Oxford University Press)

[39] Meyer G and Amer N M 1990 *Appl. Phys. Lett.* **57** 2089–91

[40] Schaffer T E 2005 *Nanotechnology* **16** 664–70

[41] Proksch R, Schaffer T E, Cleveland J P, Callahan R C and Viani M B 2004 *Nanotechnology* **15** 1344–50

[42] Ohler B 2007 *Rev. Sci. Instrum.* **78** 063701

[43] Landau L D and Lifshitz E M 1988 *Statistical Physics* (Oxford: Elsevier)

[44] Oppenheim A V and Schafer R W 1975 *Digital Signal Processing* (Englewood Cliffs, NJ: Prentise-Hall)

[45] Levy R and Maaloum M 2002 *Nanotechnology* **13** 33–7

[46] Walters D A, Cleveland J P, Thomson N H, Hansma P K, Wendman M A, Gurley G and Elings V 1996 *Rev. Sci. Instrum.* **67** 3583–90

[47] Martinez N F, Patil S, Lozano J R and Garcia R 2006 *Appl. Phys. Lett.* **89** 153115

[48] Martinez N F, Lozano J R, Herruzo E T and Garcia R 2008 *Nanotechnology* **19** 384011